Dust Emission and Molecular Depletion in L1498[1]

K. Willacy[2], W. D. Langer, T. Velusamy

Jet Propulsion Laboratory, California Institute of Technology, MS 169-506, Pasadena, CA 91109

Received ____________________; accepted ____________________

[1]Based on observations with ISO, and ESA project with instruments funded by ESA Member States (especially the PI countries: France, Germany, the Netherlands and the United Kingdom) and with the participation of ISAS and NASA.

[2]Karen.Willacy@jpl.nasa.gov

ABSTRACT

molecular cloud

We present 100 and 200μm ISOPHOT observations of the dense core L1498. We have mapped the central core by using $\Delta I_{200} = I_{200}$ - I_{100}/Θ where ΔI_{200} is a measure of the emission from the cold dust and $\Theta = I_{100}/I_{200}$ in the outer regions. The dust continuum emission provides information about the chemical depletion and the properties of cold cores where there is a lack of gas tracers. Previous observations of L1498 show that the emission from CS and CCS lie outside of the NH_3 core. The peak in ΔI_{200} lies close to the previously observed NH_3 peak. Comparison with high spatial resolution observations of $C^{18}O$ 1-0 emission show that this peaks on either side of the ΔI_{200} maximum with a dip in the core center. We estimate that the depletion factor for $C^{18}O$ in this region is at least 3 and most likely $\sim 10 - 20$. Such high depletion has significant implications for studies of gas–grain chemistry and protostellar cores.

Subject headings:

1. Introduction

L1498 is a classic example of a dense, cold, pre–protostellar core. It is extremely quiescent and shows no sign of collapse. It is very cold with a kinetic temperature of $\leq$ 10 K (Fiebig 1990, Wolkovitch et al. 1996) and lies in the Taurus Cloud Complex at a distance of 135pc. Molecular line observations have revealed an onion skin structure with CCS, CS and NH_3 (Figure 1) tracing quite different regions of the core (Kuiper et al. 1996). High spatial resolution observations of $C^{18}O$ (Lemme et al. 1995) show enhanced emission surrounding the ammonia peak and a decreased emission of $C^{18}O$ in the center of the core (where the ammonia peaks) suggesting that even this volatile molecule is depleted (see also Mezger et al. 1992). However the interpretation of depletion depends on a knowledge of the true density in the core. Since molecular line emission from traditional gas tracers, e.g. CO and CS, does not appear to be a good probe of the densest parts of this core, we have observed the 100 and 200μm dust continuum emission using ISOPHOT in order to investigate the density distribution in the center of the core.

2. Observations and data reduction

The observations were made at 100 and 200μm using the ISOPHOT C100 and C200 cameras and the standard astronomical observation template, PHT32, for raster mapping. The resultant maps are oversampled. The data were reduced using the ISOPHOT Interactive Analysis package (PIA). The integration ramps were corrected for detector non–linearities and for glitches caused by cosmic ray impacts. A first order polynomial was fitted to the ramps and the dark current removed. The data were calibrated using the internal calibration sources on ISOPHOT. The calibration is believed to be good to within a factor of two (N. Lu *private communication*).

Figure 2 (a) and (b) show the 100 and 200μm data respectively. The emission peaks in somewhat different places, indicating that the two wavelengths trace either different populations and/or different temperature distributions of dust grains. In order to investigate further we regridded the 100μm data and smoothed it to the 200μm resolution. Figure 3 plots the intensity of the 100μm data against the 200μm data. At low values of I_{100} the data can be fitted by a straight line. The departure from the linear fit at higher values where the distribution flattens out is significant. The highest values of I_{200} come from the central regions of the core and we have therefore interpreted the excess I_{200} as tracing the coldest, densest regions with the 100μm emission coming primarily from the outer layers where the gas is slightly warmer (see also Appendix A of Langer et al. 1989).

Laureijs, Clark & Prusti (1991) found a similar relationship between the 100 and 60μm IRAS data for larger scale structures in molecular clouds. The 100μm emission was found to be widespread whereas the 60μm emission was mostly outside the shielded molecular regions. We have used their method to isolate the 200μm emission from the center of L1498. We assume that outside of the core the value of $\Theta = I_{100}/I_{200}$ is approximately constant. We calculate Θ by fitting a straight line to Figure 3 (for $I_{200} < 45$ MJy/sr) and find

$$\Theta = \frac{0.1412 I_{200} + 5.025}{I_{200}} \tag{1}$$

The excess 200μm emission is then determined from

$$\Delta I_{200} = I_{200} - I_{100}/\Theta \tag{2}$$

3. Results

Figure 2 (c) shows the ΔI_{200} distribution. Its relationship to the $C^{18}O$ 1–0 line emission observed by Lemme et al. (1995) can be seen in Figure 4. The $C^{18}O$ shows two peaks with a region of lower emission in the center with a contrast of a factor of ~ 2. The dust emission peaks in between. The peak of the ΔI_{200} emission coincides with the ammonia peak seen by Kuiper et al. (1996) but not with the peaks of the other molecules (Figure 1)

3.1. Column density calculations and the depletion of $C^{18}O$

The optical depth of the 200μm emission can be calculated from

$$F_\lambda = \frac{2hc^2}{\lambda^5} \frac{1}{e^{hc/\lambda kT} - 1} \tau(\lambda) \tag{3}$$

and then the column density determined by

$$\frac{\lambda \tau(\lambda)}{N(\mathrm{H_2})} = 7 \times 10^{-27} \quad \mathrm{cm}^3 \tag{4}$$

(Draine & Lee 1984). From this the H_2 column density at the 200μm peak is calculated to be 5×10^{22} cm^{-2} assuming $T_{dust} = 10$K.

The calibration of the ISOPHOT 100 and 200μm data is uncertain to within a factor of 2. We assumed that the relative calibration of the 100 and 200μm data remains constant during the observations. In order to check our column density values we compared our results to those obtained from the $C^{18}O$ data of Lemme et al. (1995) at the $C^{18}O$ peak ($\alpha(1950) = 4^h\ 7^m\ 54^s$, $\delta(1950) = 25^\circ\ 0'\ 33''$). We used the 1–0 line in preference to the 2–1 line since it is less likely to be sensitive to excitation conditions at the densities in L1498 and it is more likely to be optically thin. The column density is given by Langer et al. (1982) as

$$N(\mathrm{C^{18}O}) = 10^{15} \int T dv \quad \mathrm{cm}^{-2} \tag{5}$$

for an excitation temperature of 10K. Assuming a fractional abundance of 1.7×10^{-7} (Frerking et al. 1982) we find that the H_2 column density inferred from the $C^{18}O$ 1–0 line, $N(\mathrm{H_2}, \mathrm{C^{18}O}\ 1\text{–}0)$, is 1.2×10^{22} cm^{-2}. The 2–1 line gives a similar column density if we use the curve of growth for $n = 10^4$ cm^{-3} in Lemme et al. (1995), which is consistent with density estimates in this region using CCS (Wolkovitch et al. 1997). At the same position $N(\mathrm{H_2},\ 200\mu\mathrm{m}) = 2.7 \times 10^{22}\ \mathrm{cm}^{-2}$ assuming $T_{dust} = 10$ K. If we assume that the $\mathrm{C^{18}O}$ is undepleted here (at the peak of the $\mathrm{C^{18}O}$ emission) then the 200μm data overestimates the column density by a factor of 2.3.

A second check on the calibration was made using the 1300μm emission which was observed at one position by Ward–Thompson et al. (1994). This gives a column density of $10^{22}\ \mathrm{cm}^{-2}$ (Lemme et al. 1995) compared to the value of $3.9 \times 10^{22}\ \mathrm{cm}^{-2}$ from the 200μm emission. Again the 200μm data yields a higher value of $N(\mathrm{H_2})$. Therefore we have rescaled ΔI_{200} by a factor of 2.3 to bring the estimate of column density into agreement with the estimate from $\mathrm{C^{18}O}$ at the $\mathrm{C^{18}O}$ peak.

At the position of the 200μm peak the $\mathrm{C^{18}O}$ emission leads to an estimate of the $\mathrm{H_2}$ column density, $N(\mathrm{H_2},\ \mathrm{C^{18}O}) = 6.5 \times 10^{21}\ \mathrm{cm}^{-2}$ compared to the rescaled $N(\mathrm{H_2},\ 200\mu\mathrm{m}) = 2.2 \times 10^{22}\ \mathrm{cm}^{-2}$. This gives a depletion factor of 3.4. However it may be higher because towards the continuum peak the $\mathrm{C^{18}O}$ emission arises partly from a halo outside of the central core ($r < 1'$). In addition our depletion estimates are likely to be low because of the differences in resolution between the 200μm and $\mathrm{C^{18}O}$ maps which would underestimate the dust column density at the 200μm peak.

To get an indication of the size of the halo effect we have made an estimate of how much of the $\mathrm{C^{18}O}$ emission comes from the core and how much from the outer regions. We assume that there is no depletion at the $\mathrm{C^{18}O}$ peak (SE position). This allows us to estimate an average density along the line of sight of $n = 4 \times 10^4\ \mathrm{cm}^{-3}$ taking the clouds depth to be equal to its semi–minor axis (0.097pc). If we assume the same depth at the 200μm peak and that the core (as traced by the 200μm emission) is 0.05pc in diameter then the core is surrounded by a shell of $\mathrm{C^{18}O}$ which is 0.024pc thick. If the average density in this layer is the same everywhere, then the outer layers contribute a $\mathrm{C^{18}O}$ column density of 9.7×10^{14} cm^{-2}. The total $C^{18}O$ column density at this point is 1.1×10^{15} cm^{-2}, leaving 1.3×10^{14} cm^{-2} as the contribution from the central core ($r < 0.05$pc). This corresponds to a H_2 column density of 8×10^{20} cm^{-2} in the central core region which is a factor of ~ 28 lower than the column density estimated from the 200μm emission. Such depletion values are also seen in protostellar disks e.g. observations of ^{13}CO in GG Tau by Dutrey et al. (1994). Our results show that similar depletion may be present in the interiors of preprotostellar cores.

3.2. Mass of the core

The virial mass of the core can be estimated using the formula given in MacLaren et al. (1988). We find that the virial mass within a sphere of radius $1'$ (corresponding to the region between the two $C^{18}O$ peaks) is 1.54 $M_\odot$, assuming $\rho \propto r^{-1}$. We have used Δv corresponding to the thermal line width for molecular hydrogen at 10 K (0.45 kms^{-1}) which is valid since the non–thermal pressure is negligible (Kuiper et al. 1996). The actual mass can be calculated using the column density derived above. We find a mass of 2.86 $M_\odot$ for the same region and an average density of $\sim 7 \times 10^4$ cm^{-3}. Since $M > M_{virial}$ the core would appear to be unstable to collapse. However if ΔI_{200} is normalized to the 1300μm data then M is reduced to 1.7 $M_\odot$, the mean density is reduced to 4×10^4 cm^{-3} and the cloud is in hydrostatic equilibrium.

3.3. Chemistry

Chemical differentiation can arise from gradients in the density, temperature or radiation field or from differences in the age of the gas. Kuiper et al. (1996) suggested that CCS traces the relatively young gas while the NH_3 traces the more evolved gas in the core center. In this picture gas is continually being added to the core from the outside.

Our 200μm results support the idea that the chemical distribution is a result of a density variation across the source. Depletion onto grains increases with density and age and is greatest in the central core where the 200μm emission peaks. Models of collapsing regions (Rawlings et al. 1992, Bergin & Langer 1997) show that the accretion of molecules onto dust in such regions can result in the preferential removal of some species while others remain in the gas phase without showing a decrease in abundance. Ammonia is a good example of a molecule whose abundance remains high even when others e.g. CO are depleted. Bergin & Langer (1997) (see their Figure 4) show how different molecules deplete at different times with CCS and CS disappearing relatively early, followed by CO and leaving NH_3 in the gas. We can therefore understand the structure of L1498 as a combination of age and density effects with young material being added to the outside of the core (Kuiper et al. 1996) and depletion increasing towards the center removing many molecules from the gas.

4. Conclusions

We have shown that the peak in the 200μm dust continuum emission coincides with the NH_3 peak and not with that of CS, CCS or $C^{18}O$. Our best estimate is that the $C^{18}O$ is depleted by a factor of $\sim 10 - 20$ in the center of the core. The 200μm emission suggests that the way the molecular lines trace different regions is a result of a density distribution with chemistry and depletion proceeding faster in the inner regions where the density is higher.

Higher spatial resolution dust continuum measurements are required to determine the details of the density distribution since the ISOPHOT beam size of $2' \times 2'$ is similar to the size of the central core. In addition observations of molecular lines predicted to remain in the gas after the onset of depletion e.g. HCO^+ and N_2H^+ would provide valuable information regarding the process of chemical depletion.

Although the depletion factor is somewhat dependent on our model assumptions and on the ISOPHOT calibration, it does not alter the fact that the 200μm emission is seen to peak in the center of the core at a point where the $C^{18}O$ emission decreases, showing that even this volatile molecule is substantially depleted.

If our depletion estimates are correct and L1498 is typical of pre–protostellar cores, then cores which are on the verge of collapse will not be visible in CO and many other molecules. Continuum studies and mapping in those molecules, e.g. NH_3, which can survive for long times even after the onset of freezeout will be required to investigate such regions. To date there have been no confirmed reports of infall being observed at the very start of collapse, prior to protostar formation. Chemical modeling of cores is required to identify which molecules are suitable tracers. It may be that the increase in density in the central core is such that most species (other than H_2 and He) are removed from the gas raising the possibility that the very early stages of collapse may be unobservable using molecular lines.

KW is a National Research Council Research Associate at the Jet Propulsion Laboratory, California Institute of Technology. This research was conducted at the Jet Propulsion Laboratory, California Institute of Technology under support from the National Aeronautics and Space Administration. We would like to thank Dr. N. Lu of IPAC for his help and advice regarding reduction of the ISOPHOT data.

The ISOPHOT data presented in this paper was reduced using PIA, which is a joint development by the ESA Astrophysics Division and the ISOPHOT consortium. The ISOPHOT consortium is led by the Max Planck Institute for Astronomy (MPIA), Heidelberg. Contributing ISOPHOT consortium institutes are DIAS, RAL, AIP, MPIK and MPIA.

REFERENCES

Bergin, E. A., Langer, W. D. 1997, ApJ, 486, 328

Draine, B. T., Lee, H. M. 1984, ApJ, 285, 89

Dutrey, A., Guilloteau, S., Simon, M. 1994, A&A, 286, 149

Fiebig, D. 1990, Ph.D. thesis, Univ. Bonn

Frerking, M. A., Langer, W. D., Wilson, R. W. 1982, ApJ, 262, 590

Kuiper, T. B. H., Langer, W. D., Velusamy, T. 1996, ApJ, 468, 761

Langer, W. D., Wilson, R. W., Goldsmith, P. F., Beichman, C. A. 1989, ApJ, 337, 355

Laureijs, R. J., Clark, O. F., & Prusti, T. 1991, ApJ, 372, 185

Lemme, C., Walmsley, C. M., Wilson, T. L., Muders, D. 1995, A&A, 302, 509

MacLaren, I., Richardson, K. M., Wolfendale, A. W. 1988, ApJ, 333, 821

Mezger, P. C., Sievers, A., Zylka, R., Haslam, C. G. T., Kreysa, E., Lemke, R. 1992, A&A, 265, 743 Rawlings, J. M. C., Hartquist, T. W., Menten, K. M., Williams, D. A. 1992, MNRAS, 255, 471

Ward–Thompson, D., Scott, P. F., Hills, R. E., André, P. 1994, MNRAS, 268, 276

Wolkovitch, D., Langer, W. D., Goldsmith, P. F., Heyer, M. 1996, ApJ, 477, 241

This manuscript was prepared with the AAS LaTeX macros v4.0.

Fig. 1.— The structure of the L1498 core as traced by CS, CCS and NH_3 emission (adapted from Kuiper et al. 1996). The single dish CCS and NH_3 data are shown by the light and heavy dash–dot lines. The CS data from OVRO is indicated by the solid lines and the grey scale shows the combined VLA and DSN u–v reconstruction of the CCS emission.

Fig. 2.— The continuum emission at (a) 100μm (with contours at intervals of 0.25 MJy/sr between 9 and 12 MJy/sr) and (b) 200μm (with contours at intervals of 2 MJy/sr between 32 and 54 MJy/sr). Panel (c) shows the results of the subtraction process and reveals the coldest parts of the core. The contours in (c) run from 0.5 to 5.5 MJy/sr at 0.5 MJy/sr intervals. The center of each map is at RA(1950) = $4^h\ 7^m\ 49.62^s$, dec(1950) = $25^\circ\ 2'\ 2.6''$.

Fig. 3.— A scatter plot of the 100μm data vs. the 200μm data showing the two regimes of dust emission. The 100μm emission flattens out at high values of I_{200} which we have taken to indicate that the 100μm emission traces slightly warmer dust with the 200μm emission also tracing the colder dust in the center of the core. The solid line indicates the fit to the data used to remove the contribution from the warm dust from the 200μm data to leave the emission from the coldest dust.

Fig. 4.— The very cold dust in the center of L1498 as traced by $\Delta I_{200} = I_{200}$ - I_{100}/Θ (dashed lines) superimposed on the $C^{18}O$ 1–0 emission from Lemme et al. (1995) (solid lines). The 200μm central contours are at 4.0, 4.5, 5.0 and 5.5 MJy/sr. The outer contour traces the boundary of ΔI_{200} at 0.5 MJy/sr. The intermediate contours have been omitted for clarity, see Figure 2(c) for the complete map. For $C^{18}O$ the contours are at intervals of 0.1 $Kkms^{-1}$ between 0.7 and 1.8 $Kkms^{-1}$. The I_{200} μm emission can be seen to peak at the central dip in the $C^{18}O$ emission. The center of the map is at $25^\circ\ 1'\ 33''$.

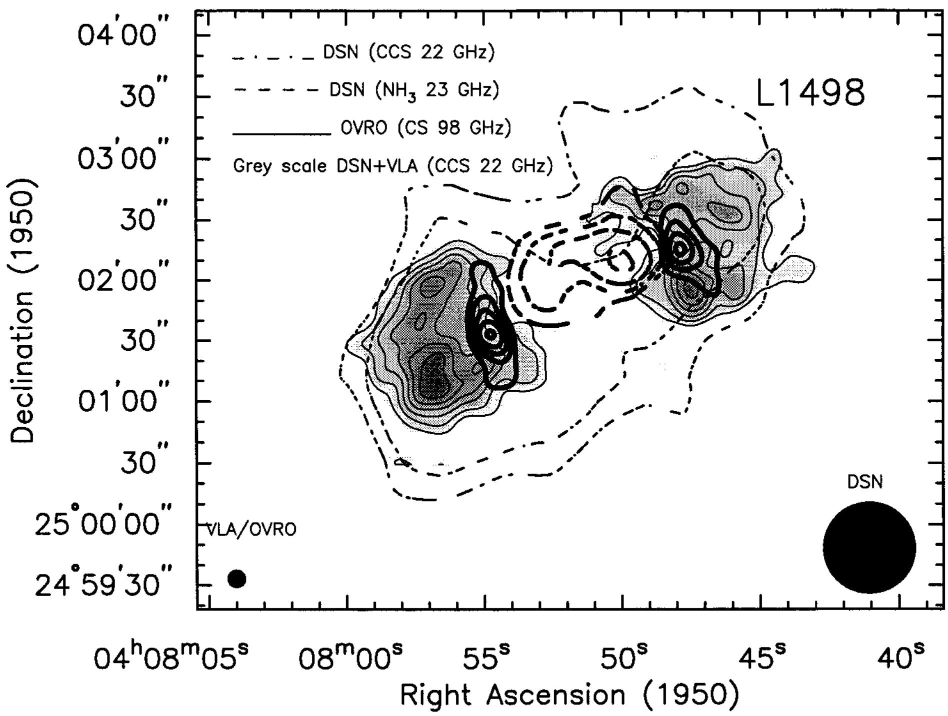
DSN (CCS 22 GHz)
DSN (NH_3 23 GHz)
OVRO (CS 98 GHz)
Grey scale DSN+VLA (CCS 22 GHz)
L1498
Declination (1950)
04′00″
30″
03′00″
30″
02′00″
30″
01′00″
30″
25°00′00″
24°59′30″
VLA/OVRO
DSN
04h08m05s
08m00s
55s
50s
45s
40s
Right Ascension (1950)

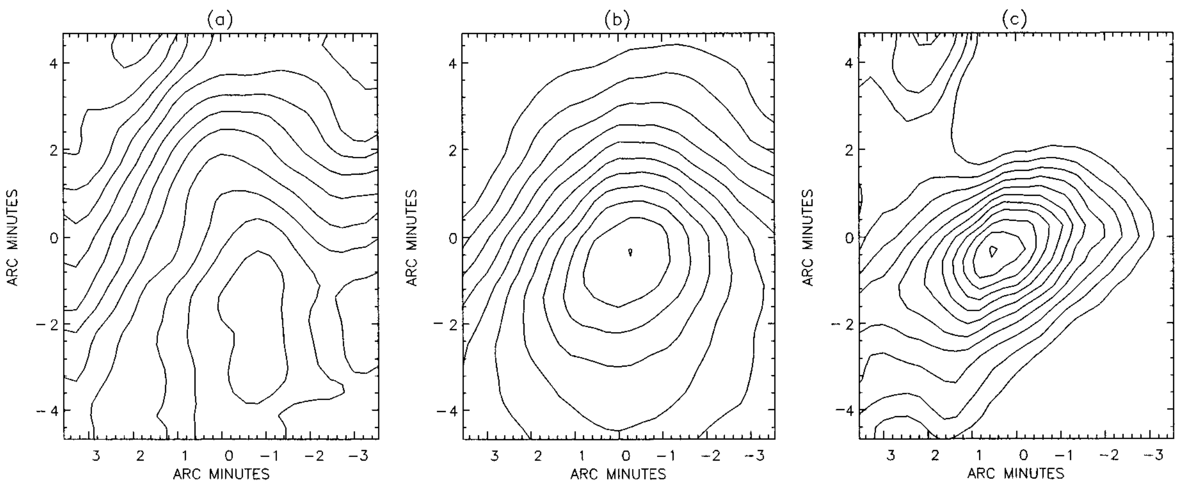
(a)
(b)
(c)
ARC MINUTES
ARC MINUTES
ARC MINUTES
ARC MINUTES
ARC MINUTES
ARC MINUTES

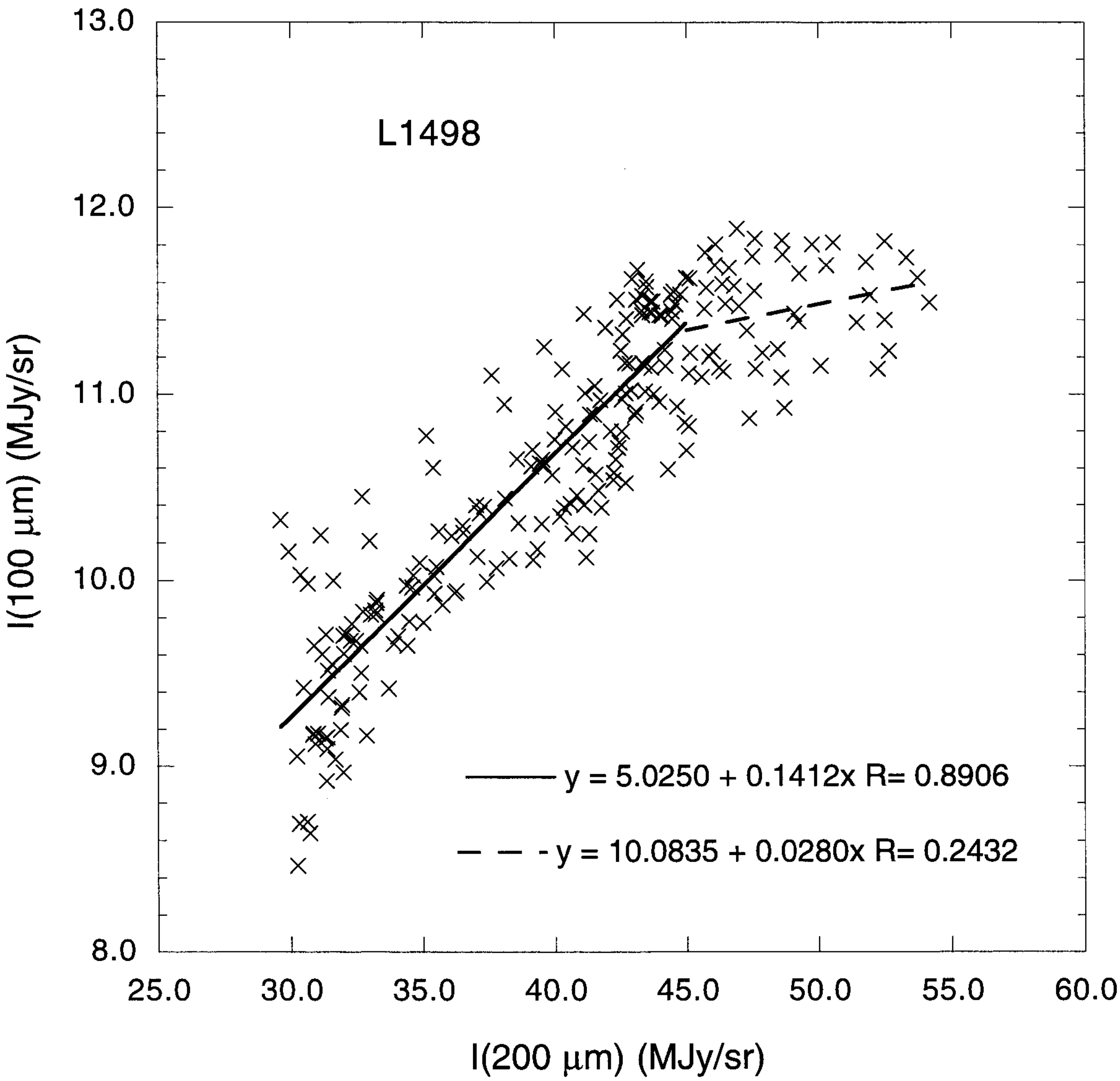
L1498
y = 5.0250 + 0.1412x R= 0.8906
y = 10.0835 + 0.0280x R= 0.2432
I(100 μm) (MJy/sr)
I(200 μm) (MJy/sr)
13.0
12.0
11.0
10.0
9.0
8.0
25.0
30.0
35.0
40.0
45.0
50.0
55.0
60.0

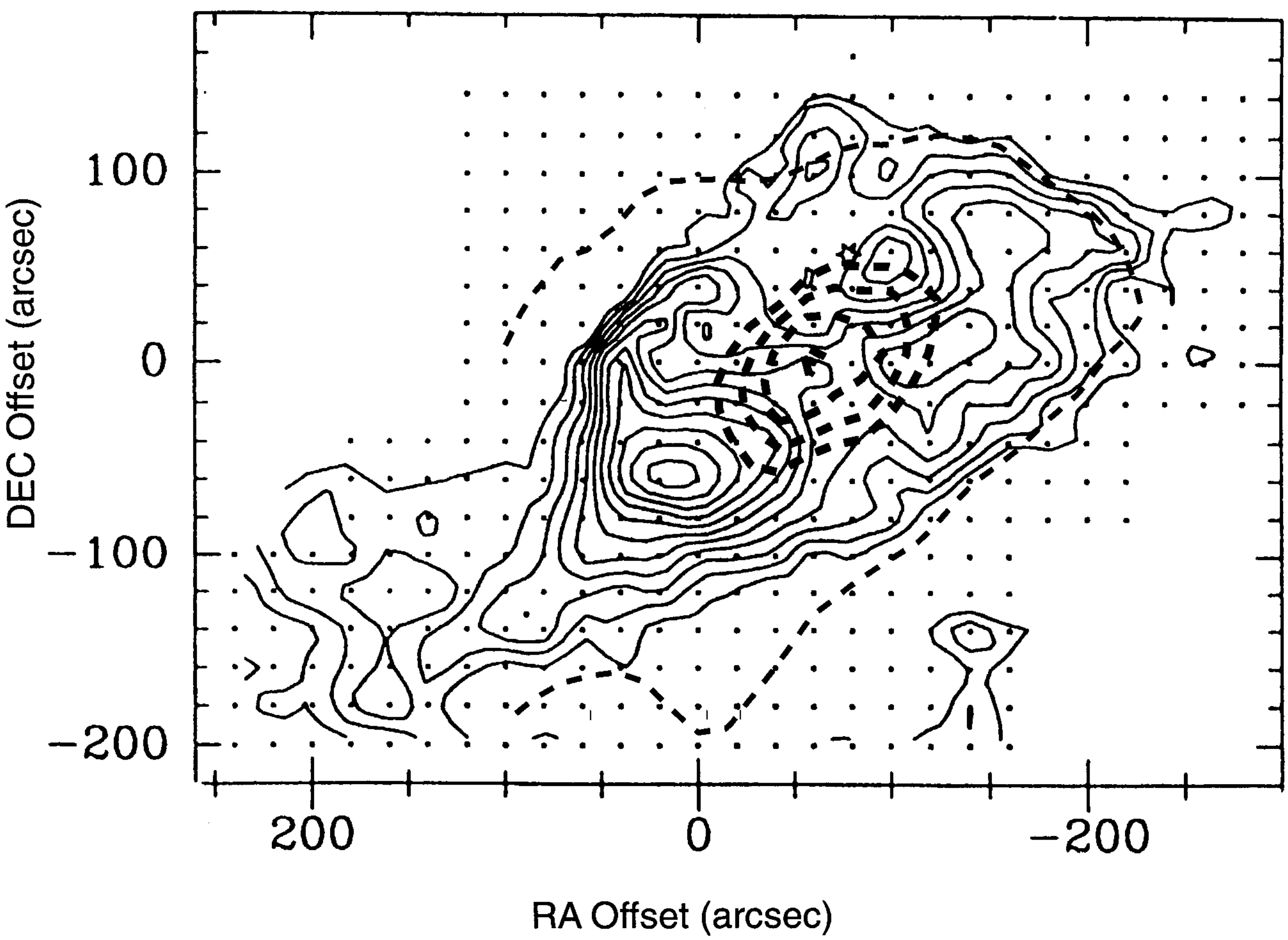
100
0
−100
−200
DEC Offset (arcsec)
200
0
−200
RA Offset (arcsec)